

# Constitutive modelling of carbon fibre reinforced polymers for adhesively bonded cfrp-steel joints

Michael Donhauser<sup>1</sup> and Anton Matzenmiller<sup>\*,1</sup>

<sup>1</sup>Institute of Mechanics, Dept. of Mechanical Engineering, University of Kassel, Mönchebergstr. 7, 34125 Kassel, Germany

---

**Abstract.** This contribution comprises the constitutive modelling and finite element failure analysis of adhesively bonded cfrp-steel joints under quasi-static loading with the focus on the modelling of the cfrp. A transversely isotropic material model is utilised for the elastic-brittle behaviour of the cfrp, where a nonlinear ansatz takes the axial shear behaviour into account. The inter-fibre failure and postcritical behaviour of the cfrp are modelled by PUCK's failure criterion and a failure mode based anisotropic damage approach. Delamination is considered by means of an interface model with a bilinear traction-separation-law. The adhesive layer is characterised by the so-called Toughened-Adhesive-Polymer (TAPO) model, for elasto-plasticity and isotropic damage. An elasto-plastic material model is used for the steel components. For four of the six test cases, the numerical validation results under quasi-static loading show a good agreement with the test data.

---

## 1 Introduction

Today, material compounds with enhanced mechanical properties are made of carbon fibre reinforced polymers (cfrp) and steel components by means of adhesive joining. In order to optimise the structural strength of the material compound with the finite element method, material models must be used that capture the elastic and failure behaviour of each individual material accurately. Especially, the failure modelling of cfrp is a challenging task due to the complex failure mechanisms and the interaction of different failure modes causing ultimate fracture. In [6], material models, which are implemented in the commercial FE-software LS-DYNA, are used to perform FE-simulations for cfrp and adhesive-cfrp-steel joints that exhibit a simple stress state. The lack of capturing the nonlinear axial shear behaviour as well as the postcritical behaviour after a first ply failure, leads to improvable results. Therefore, in [7], a detailed model for the cfrp is developed, which captures the nonlinear axial shear behaviour, the intralaminar failure due to fibre and inter-fibre breakage, the postcritical behaviour after a first ply failure and the interlaminar failure i. e. delamination. The constitutive model of the cfrp is presented in this contribution.

## 2 Constitutive Modelling

### 2.1 Carbon Fibre Reinforced Polymer

The elastic material behaviour of the unidirectional layer (ud-layer), depicted in Fig. 1, is described by the transverse isotropic model. The model is formulated in the material coordinate system  $(x_1, x_2, x_3)$ , where  $x_1$  denotes the fibre direction. For the normal strain the strain-stress relation reads as

$$\begin{Bmatrix} \varepsilon_{11} \\ \varepsilon_{22} \\ \varepsilon_{33} \end{Bmatrix} = \begin{bmatrix} \frac{1}{E_1} & -\frac{\nu_{12}}{E_1} & -\frac{\nu_{12}}{E_1} \\ & \frac{1}{E_2} & -\frac{\nu_{23}}{E_2} \\ \text{sym.} & & \frac{1}{E_2} \end{bmatrix} \begin{Bmatrix} \sigma_{11} \\ \sigma_{22} \\ \sigma_{33} \end{Bmatrix}, \quad (1)$$

whereby  $E_1$  is the YOUNG'S modulus in fibre direction,  $E_2$  perpendicular to the fibre direction and  $\nu_{12}$  is the POISSON'S ratio in the coordinate direction  $x_1x_2$ . The transverse shear behaviour is described with the transverse shear modulus  $G_{23}$  by the linear ansatz:

$$\tau_{23} = G_{23}\gamma_{23} \quad \text{with} \quad G_{23} = \frac{E_2}{2(1 + \nu_{23})}, \quad (2)$$

---

\*Corresponding author: e-mail post-structure@uni-kassel.de, phone +49 (0)561 804 2043, fax +49 (0)561 804 2720

and the axial shear behaviour by the nonlinear ansatz with the model parameters  $c_0$ - $c_3$ :

$$\tau_{1j}(\gamma_{1j}) = c_0 \tanh(c_1 \gamma_{1j}) + c_2 \tanh(c_3 \gamma_{1j}) \quad j = 2, 3 \quad . \quad (3)$$

**Failure model** The intralaminar failure of the cfrp is divided into inter-fibre and fibre failure. In PUCK's exposure criterion, the normal stress  $\sigma_n$  and shear stress  $\tau_{nt}$  and  $\tau_{n1}$  acting on the potential fracture plane, which is inclined about the fracture angle  $\theta_{fp}$  (see Fig. 1), are used to describe the inter-fibre failure in an ud-layer. For tensile loading ( $\sigma_n \geq 0$ ) the exposure criterion reads as

$$f_E^+(\theta_{fp}) = \sqrt{\left(\frac{1}{R_{\perp}^+} - \frac{p_{\perp\psi}^+(\theta_{fp})}{R_{\perp\psi}^+} \right)^2 \sigma_n^2(\theta_{fp}) + \left(\frac{\tau_{nt}(\theta_{fp})}{R_{\perp\perp}^+} \right)^2 + \left(\frac{\tau_{n1}(\theta_{fp})}{R_{\perp\parallel}^+} \right)^2} + \frac{p_{\perp\psi}^+(\theta_{fp})}{R_{\perp\psi}^+} \sigma_n(\theta_{fp}) = 1 \quad (4)$$

and for compressive loading ( $\sigma_n < 0$ ) as

$$f_E^-(\theta_{fp}) = \sqrt{\left(\frac{\tau_{nt}(\theta_{fp})}{R_{\perp\perp}^-} \right)^2 + \left(\frac{\tau_{n1}(\theta_{fp})}{R_{\perp\parallel}^-} \right)^2 + \left(\frac{p_{\perp\psi}^-(\theta_{fp})}{R_{\perp\psi}^-} \sigma_n(\theta_{fp}) \right)^2} + \frac{p_{\perp\psi}^-(\theta_{fp})}{R_{\perp\psi}^-} \sigma_n(\theta_{fp}) = 1 \quad . \quad (5)$$

In Eqs. (4)-(5) all quantities  $R^A$  are fracture resistances acting on the action plane A and all  $p^\pm$  are slope parameters of failure envelopes, see [8] for details. The fracture stresses are functions of the global stress state and the fracture angle  $\theta_{fp}$ :

$$\sigma_n(\theta_{fp}) = c^2 \sigma_{22} + s^2 \sigma_{33} + 2cs\tau_{23}, \quad \tau_{nt}(\theta_{fp}) = -s\sigma_{22} + s\sigma_{33} + (c^2 - s^2)\tau_{23}, \quad \tau_{n1}(\theta_{fp}) = c\tau_{12} + s\tau_{13} \quad (6)$$

with  $c = \cos(\theta_{fp})$  and  $s = \sin(\theta_{fp})$ . The fibre stress  $\sigma_{11}$  does not influence the inter-fibre failure and is therefore neglected in Eq. (6). In order to evaluate the exposure criterion, it is always necessary to determine the fracture angle  $\theta_{fp}$  for a given stress state ( $\sigma_{22}, \sigma_{33}, \tau_{12}, \tau_{23}, \tau_{13}$ ). The fracture angle is defined as that one, for which the exposure criterion reaches the maximum value. Hence, for tension ("+" ) or compression ("-") we solve the corresponding nonlinear scalar equation

$$\frac{\partial f_E^\pm(\theta_{fp})}{\partial \theta_{fp}} = 0 \quad \text{with} \quad \theta_{fp} \in [-90^\circ, 90^\circ] \quad (7)$$

using Newton's method. The obtained fracture angle from (7) and corresponding stress state from (6) are used to evaluate the exposure criterion (4) or (5), while an inter-fibre failure occurs if  $f_E^\pm \geq 1$ .

The fibre failure under tensile loading is taken into account by the maximum stress criterion

$$f_{fb} = \frac{\sigma_{11}}{R_{\parallel}} = 1 \quad \text{with} \quad R_{\parallel} : \text{tensile fibre strength} \quad . \quad (8)$$

**Post-critical behaviour** In a multidirectional laminate, first ply failure due to an inter-fibre breakage does not lead to abrupt loss of load-bearing. The load-bearing capacity is still remaining, but with a reduced laminate stiffness. In this contribution, a failure mode based anisotropic damage approach with six damage variables is applied to capture the stiffness reduction according to [4]. A  $3 \times 3$  damage operator with the damage variables  $\omega_{11}, \omega_{22}$  and  $\omega_{33}$  arranged along the major diagonal, is introduced and applied to Eq. (1) in order to obtain the compliance relationship in terms of the damage variables:

$$\begin{Bmatrix} \varepsilon_{11} \\ \varepsilon_{22} \\ \varepsilon_{33} \end{Bmatrix} = \begin{bmatrix} \frac{1}{(1-\omega_{11})E_1} & -\frac{\nu_{12}}{E_1} & -\frac{\nu_{13}}{E_1} \\ \frac{1}{(1-\omega_{22})E_2} & -\frac{\nu_{23}}{E_2} & \\ \text{sym.} & \frac{1}{(1-\omega_{33})E_3} & \end{bmatrix} \begin{Bmatrix} \sigma_{11} \\ \sigma_{22} \\ \sigma_{33} \end{Bmatrix} \quad . \quad (9)$$

The proposed method of [5] is applied to the components of the minor diagonal in Eq. (9) to retain the symmetry of the compliance matrix. In case of damage, the linear and nonlinear ansatz of the shear behaviour in Eq. (2) and (3) reads as:

$$\tau_{23} = (1 - \omega_{23})G_{23}\gamma_{23} \quad , \quad \tau_{1j} = (1 - \omega_{1j})(c_0 \tanh(c_1 \gamma_{1j}) + c_2 \tanh(c_3 \gamma_{1j})) \quad j = 2, 3 \quad . \quad (10)$$

The Eqs. (4),(5) and (8) are used to define the loading functions

$$f_2^\pm = f_E^\pm - r_2^\pm = 0 \quad \text{and} \quad f_1 = f_{fb} - r_1 = 0 \quad (11)$$

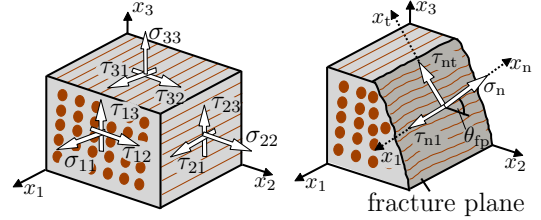


**Figure 1.** Ud-layer with stress state on fracture plane

with the variable thresholds

$$r_2^\pm = \max\left[1, \max_{-\infty < \tau < t} (f_E^\pm)\right] \quad \text{and} \quad r_1 = \max\left[1, \max_{-\infty < \tau < t} (f_{fb})\right] \quad (12)$$

due to inter-fibre and fibre failure, respectively. For  $f_2^\pm < 0$  and  $f_1 < 0$  there is no damage evolution, thus  $r_2^\pm = 1$  and  $r_1 = 1$ . With the damage growth functions for the corresponding failure mode

$$\phi_2^\pm = 1 - \exp\left[\frac{1 - (r_2^\pm)^{m_2}}{m_2}\right] \quad \text{and} \quad \phi_1 = 1 - \exp\left[\frac{1 - (r_1)^{m_1}}{m_1}\right] \quad (13)$$

the damage evolution is defined as

$$\boldsymbol{\omega} = \phi_1 \mathbf{l} + \phi_2 \mathbf{q} \quad (14)$$

with  $\boldsymbol{\omega} = [\omega_{11}, \omega_{22}, \omega_{33}, \omega_{12}, \omega_{23}, \omega_{13}]^T$ ,  $\mathbf{l} = [l_{22}, l_{33}, l_{12}, l_{23}, l_{13}]^T$  and  $\mathbf{q} = [0, q_{22}, q_{33}, q_{12}, q_{23}, q_{13}]^T$ . In Eq. (13), the quantities  $m_2$  and  $m_1$  denote the strain softening parameters. The components of  $\mathbf{l}$  and  $\mathbf{q}$  in Eq. (14) are parameters, which enable the coupling of the individual damage variables. In brittle multidirectional laminates, which are considered in this contribution, abrupt and ultimate failure occurs, when the fibre failure criterion in Eq. (8) is reached, thus  $\phi_1$  in Eq. (14) is zero. The presented constitutive equations for the cfrp are implemented as a user defined material model in LS-DYNA.

**Delamination** In order to describe the delamination process, interface elements are used in combination with the interface model Cohesive-Mixed-Mode (\*Mat\_138) from LS-DYNA, which includes a bilinear traction-separation-law and a quadratic mixed mode criterion according to [3]. The model parameters are identified from test data of fracture mechanical DCB- and ENF-specimens.

## 2.2 Adhesive Layer and Steel Components

The adhesive layer is characterised by the so-called TAPO-model, which is an elasto-plastic model with damage. More details about this material model can be found in [1] and [2].

The material behaviour of the steel is described by the simple model Piecewise-Linear-Plasticity (\*Mat\_24) from LS-DYNA together with stress-strain test data of the steel at hand. The element deletion method is applied, when the equivalent strain reaches the defined failure value.

## 3 Validation

The FE-simulation and failure analysis is carried out for the so-called thin shear specimen, depicted in Fig. 2. The specimen consists of a steel adherend and a quasi-isotropic laminate, which are bonded together by the adhesive layer. The quasi-isotropic laminate has 13 plies and an overall thickness of 2 mm. The thin shear specimen is tested for three adhesive thicknesses ( $d_k=0.3, 1$  and 2 mm) and two laminate orientation ( $0^\circ$  and  $90^\circ$ ) in order to investigate their influence on the failure behaviour.

For the laminate orientation of  $0^\circ$  the layup configuration is  $[0^\circ, 90^\circ, +45^\circ, -45^\circ, 0^\circ, 90^\circ, +45^\circ, 90^\circ, 0^\circ, -45^\circ, +45^\circ, 90^\circ, 0^\circ]$ , whereby the fibre direction of the top layer, which is attached to the adhesive, coincides with the loading direction, see Fig. 2. In the case of the  $90^\circ$  orientation, the fibres in the top layer are arranged perpendicular to the loading direction leading to the layup configuration  $[90^\circ, 0^\circ, -45^\circ, +45^\circ, 90^\circ, 0^\circ, -45^\circ, 0^\circ, 90^\circ, +45^\circ, -45^\circ, 0^\circ, 90^\circ]$ . Each of the thirteen single layers is discretised by a three-dimensional solid element in the FE-model, where interface elements are placed between adjacent layers to take delamination into consideration. In the FE-simulation, failure can occur in the adhesive layer, the steel component or in the laminate in form of a fibre breakage, an inter-fibre fracture or a delamination.

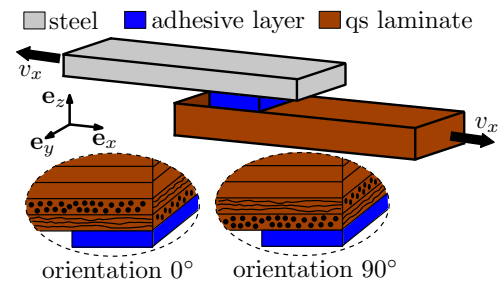


**Figure 2.** Sketch of thin shear specimen with different laminate orientations

The material parameters are identified from test data of individual specimens of each material. The identification procedure and all identified parameters are documented in [7] in detail. In Fig. 3, the numerical and experimental results are shown for a quasi-static loading ( $v = 1$  mm/min). In four of six test cases the numerically obtained stress-strain-curves correspond well with the experiments, see Fig. 3 a, b, d, f. The structural strength is slightly and the failure strain strongly underestimated for the both other cases (Fig. 3 c, e). For the laminate orientation of  $90^\circ$  in the test and in the simulation, failure occurs always

in the laminate due to delamination between the first and second ply caused by an preceding inter-fibre breakage in the top layer, see Fig 3 for instance. In the test, failure in the adhesive layer occurs for the laminate orientation of  $0^\circ$  and the adhesive thickness of  $d_k = 0.3$  and 1 mm. The FE-calculation predicts the correct failure mode for the thinner adhesive layer. The test results of the specimen with  $d_k = 2$  mm and laminate orientation  $0^\circ$  shows mixed failure in the adhesive layer and laminate, where the simulation predicts only failure in the laminate. The validation results under quasi-static loading show that with the presented method four of the six force-displacement-curves with the corresponding failure mode are reproduced well. In both other cases (Fig. 3 c, e), the deviation in the force-displacement-curves is caused by premature delamination in the FE-simulation, which will be part of forthcoming investigations.

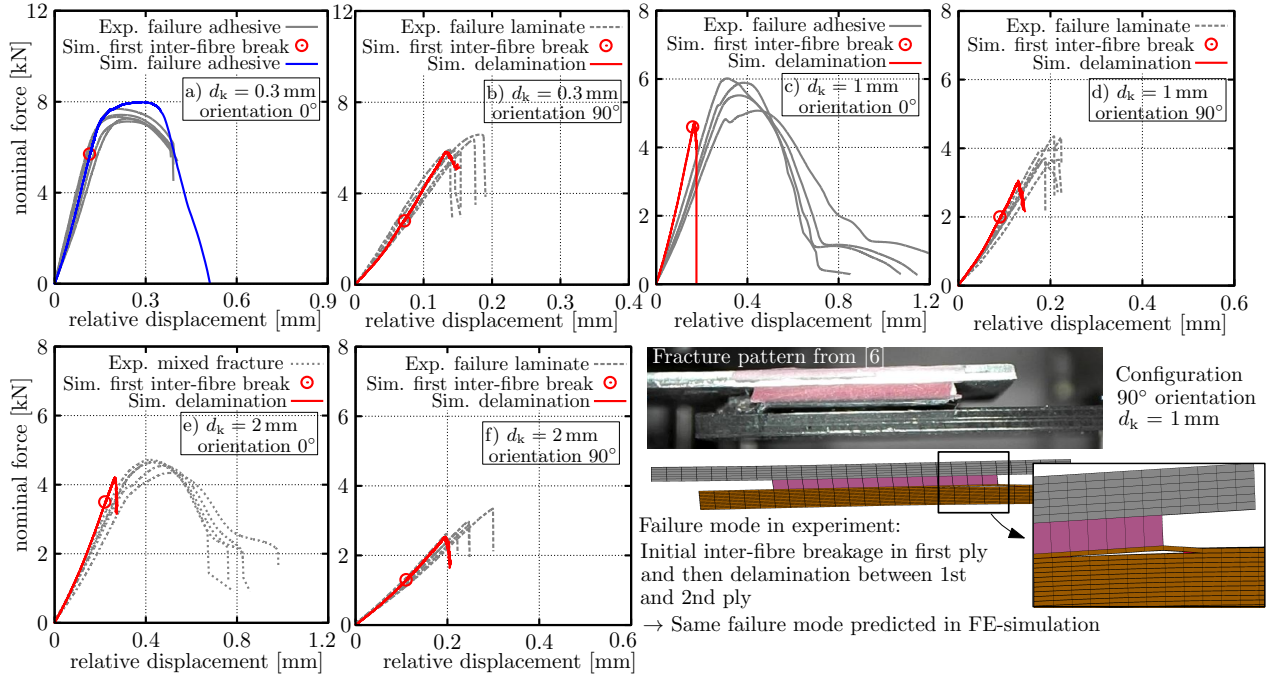


**Figure 3.** Validation results of adhesively bonded thin shear specimen with steel adherend and quasi-isotropic laminate

## References

- [1] W. Böhme, M. Brede, F. Burbulla, C. Fehrenbach, O. Hesebeck, S. Kilchert, J. Lienhard, R. Mahnken, S. Marzi, A. Matzenmiller, Michael May, D. Memhard, N. Nörenberg, L. Reissig, and H. Voß. *Robustheit und Zuverlässigkeit der Berechnungsmethoden von Klebverbindungen mit hochfesten Stahlblechen unter Crashbedingungen*. Abschlussbericht, FOSTA-Forschungsvereinigung. 2013.
- [2] M. Brede, F. J. Heise, M. Schlimmer, A. Matzenmiller, R. Mahnken, O. Hahn, K. Dilger, P. Gumbsch, K. Thoma, and O. D. Hennemann. *Methodenentwicklung zur Berechnung von höherfesten Stahlklebverbindungen des Fahrzeugbaus unter Crashbelastung*. Abschlussbericht, FOSTA-Forschungsvereinigung. 2008.
- [3] Pedro P. Camanho and Carlos G. Dávila. Mixed-mode decohesion finite elements for the simulation of delamination in composite materials (2002).
- [4] M. Chatiri and A. Matzenmiller. A Damage-Mode Based Three Dimensional Constitutive Model for Fibre-Reinforced Composites. *CMC: Computers, Materials & Continua* 35.3 (2013), pp. 255–283.
- [5] A. Matzenmiller, J. Lubliner, and R. L. Taylor. A constitutive model for anisotropic damage in fiber-composites. *Mechanics of materials* 20.2 (1995), pp. 125–152.
- [6] G. Meschut, M. Wünsche, A. Matzenmiller, and M. Schmerbauch. *Beanspruchungs- und fertigungsgerechtes Kleben von Faserverbundkunststoffen im Multi-Material-Design*. Abschlussbericht, Forschungsvereinigung Stahlanwendung FOSTA. 2015.
- [7] G. Meschut, K. Henkel, A. Matzenmiller, and M. Donhauser. *Experimentelle und numerische Untersuchungen zum Versagensverhalten von kalt ausgehärteten Stahl-FVK-Klebverbindungen unter schlagartiger Belastung*. Abschlussbericht, Forschungsvereinigung DECHEMA. 2018.
- [8] A. Puck. *Festigkeitsanalyse von Faser-Matrix-Laminaten: Modelle für die Praxis*. Hanser, 1996.